

This work was written as part of one of the author's official duties as an Employee of the United States Government and is therefore a work of the United States Government. In accordance with 17 U.S.C. 105, no copyright protection is available for such works under U.S. Law.

Public Domain Mark 1.0

<https://creativecommons.org/publicdomain/mark/1.0/>

Access to this work was provided by the University of Maryland, Baltimore County (UMBC) ScholarWorks@UMBC digital repository on the Maryland Shared Open Access (MD-SOAR) platform.

Please provide feedback

Please support the ScholarWorks@UMBC repository by emailing scholarworks-group@umbc.edu and telling us what having access to this work means to you and why it's important to you. Thank you.

Look Angle Correction for SMAP L-Band Radiometer Using Geolocation Measurements

David. M. Le Vine¹, *Life Fellow, IEEE*, Emmanuel P. Dinnat², *Senior Member, IEEE*, Paolo de Matthaeis³, *Senior Member, IEEE*, and Jinzheng Peng⁴, *Senior Member, IEEE*

Abstract—Geolocation of the radiometer footprint in scanning instruments such as soil moisture active passive (SMAP) has been successfully demonstrated using the change in antenna temperature as the radiometer scans across land/water boundaries (coastlines). This measurement provides the distance of the footprint from the nominal coastline, but it does not provide information about the error in look angle and azimuth of the antenna boresight vector needed to correct the geolocation error. A method for doing this is reported using fore and aft crossings of the boundary. The approach is demonstrated using the SMAP radiometer simulator and then applied to SMAP data over the west coast of Madagascar. The error estimates of 0.3° for the look angle and 0.15° for azimuth are consistent with independent estimates.

Index Terms—Geolocation, microwave radiometer, remote sensing.

I. INTRODUCTION

CONFIRMING the location on the surface of the footprint of a remote sensing instrument in space (geolocation) is an important step in delivering accurate data. This is particularly important for instruments at L-band such as SMAP (Soil Moisture Active Passive) which employ large antennas with patterns that are hard to measure accurately prior to launch. The large contrast between land and water at L-band (about 150 K) makes coastlines an ideal landmark to use in geolocation. In scanning instruments such as SMAP, it is possible to use the characteristic change in antenna temperature, TA, as the radiometer scans across a land-water boundary to locate the boundary with accuracy much better than the size of the instrument's footprint. For example, [1] used the inflection point in the change in TA as the radiometer scanned across selected coastlines of Madagascar, Australia, and elsewhere to confirm the pointing of the SMAP antenna boresight to within about 2 km even though the radius of the radiometer footprint is on the order of 40 km.

Manuscript received 7 March 2024; revised 16 April 2024; accepted 21 May 2024. Date of publication 29 May 2024; date of current version 10 June 2024. (Corresponding author: David. M. Le Vine.)

David. M. Le Vine and Emmanuel P. Dinnat are with the NASA Goddard Space Flight Center, Greenbelt, MD 20771 USA (e-mail: david.m.levine@nasa.gov; emmanuel.dinnat@nasa.gov).

Paolo de Matthaeis is with the Cryospheric Sciences Laboratory, NASA Goddard Space Flight Center, Greenbelt, MD 20771 USA, and also with the University of Maryland at Baltimore, Baltimore, MD 21250 USA (e-mail: paolo.demathaeis@nasa.gov).

Jinzheng Peng is with the NASA Goddard Space Flight Center, Greenbelt, MD 20771 USA, and also with Morgan State University, Baltimore, MD 21251 USA (e-mail: jinzheng.peng@nasa.gov).

Digital Object Identifier 10.1109/TGRS.2024.3405811

Le Vine et al. [2] used the fourth Stokes parameter, which is zero almost everywhere at L-band but has spikes at land-water boundaries, to achieve similar accuracy along the western coastline of Madagascar.

However, verifying the accuracy of geolocation is only part of the problem of determining accuracy in remote sensing. Providing accurate measurements of soil moisture and/or ocean salinity (two of the major science products at L-band) requires accurate knowledge of the incidence angle at the surface; while knowledge of the geolocation error puts bounds on errors in the knowledge of the antenna boresight vector, it does not directly provide the boresight vector itself (e.g., polar coordinates relative to nadir) or information on how to correct the error in the incidence angle at the surface associated with the geolocation error.

In recent work, Peng et al. [3] used data similar to that employed by [1] to look for the change in spacecraft attitude (pitch, roll, and yaw) that would minimize the geolocation error. This analysis yielded small changes in attitude that would significantly reduce the mean error. However, these parameters are not unique, and it is not clear that the error in antenna look angle obtained in this way is the one needed in the science retrieval algorithm.

In this manuscript, it is shown that the scan across coastlines can also be used to identify the errors in the look angle (θ) and azimuth (φ) of the antenna boresight vector associated with the geolocation error. The starting point is the change in antenna temperature as the footprint crosses a land/water boundary, using the procedure previously adopted for geolocation [2], [1] to locate the footprint relative to the coastline. It is shown that the error manifests as a yaw error (an azimuth error) but with a pattern that depends on the orientation of the scan with respect to the surface. With knowledge of this geometry, and by comparing crossings in the forward and aft portions of the scan, it is possible to separate azimuth and look for angle error. The technique is demonstrated with numerical simulation and then applied to SMAP data over the coastline of Madagascar. The analysis over Madagascar indicates a small error in pointing that is consistent with results obtained by an independent technique over the ocean using GNSS-R [4].

II. BACKGROUND

A. Soil Moisture Active Passive

The SMAP radiometer employs a conically scanned antenna and operates in the microwave band at 1.413 GHz protected

for passive use only. The antenna scan has a cone angle of 35.5° about the spacecraft Z-axis (pointing perpendicular to the surface) with a scan rate of 14.6 r/min [5], [6]. At the spacecraft's altitude of 685 km, the incidence angle at the ground is 40° and the 3 dB footprint on the surface is about 39×47 km [5]. The radiometer is fully polarimetric (i.e., it measures the four modified Stokes parameters, TaV, TaH, Ta3, and Ta4 [7] and after the frontend filter and amplification, the processing is digital and coherent [6], [8]. The radar on SMAP stopped transmitting very soon after launch in 2015.

The fundamental datum of the radiometer is a measurement averaged over an integration time of 0.3 ms and bandwidth of 24 MHz. The data in each 0.3 ms are sampled at a rate of 96 Msamples/s [8]. The measurement is coherent (phase and amplitude are preserved) and the moments of the data are computed including the second moment at each polarization (i.e., TaV and TaH) and the real and imaginary part of the cross correlation between the two polarizations (i.e., Ta3 and Ta4). This basic measurement is repeated every 0.35 ms (there is a gap of 0.05 ms between measurements which was assigned to the radar). The data are grouped into “packets” of four measurements each, and four packets of science data are followed by two packets for calibration and housekeeping data. This is repeated twice to form a “footprint,” which is the basic unit for science data [5], [6].

B. Geolocation

Geolocation of the footprint of the SMAP radiometer was checked soon after launch by [1] using the characteristic shape of the antenna temperature, TA, as the radiometer antenna scanned across land-water boundaries (i.e., coastlines). At L-band the contrast between land and water is very large (on the order 150 K) and the transition between land and water has a characteristic shape which for a reasonably straight coastline is close to the convolution of the antenna pattern with a step-function. The inflection point in this transition is a good indicator of the location of the boundary [2].

This process is illustrated in Fig. 1. The panel on the top shows the track of a SMAP scan across the eastern coastline of Madagascar during descending orbit 01470 D. The footprints used for geolocation (13 in this example) are indicated with a “+.” The panel on the bottom is a plot of the antenna temperature at vertical polarization, TaV, from these footprints. The solid curve is a fit to TaV using a fourth-order polynomial. In the ideal case (no noise and a step function boundary), it can be shown that the inflection point of this curve is an accurate indicator of the location of the boundary (e.g., see [2, Appendix A]) and that the accuracy with which the boundary can be located is not limited by the resolution of the antenna. Amici et al. [1], using a variation of this approach (the method for fitting to the data was different), reported an accuracy of 2 km whereas the resolution of the SMAP antenna is on the order of 40 km.

It is also possible to use the peak in the fourth Stokes vector, Ta4, which occurs over scenes with mixed brightness temperatures to locate the boundary [2]. This is illustrated in

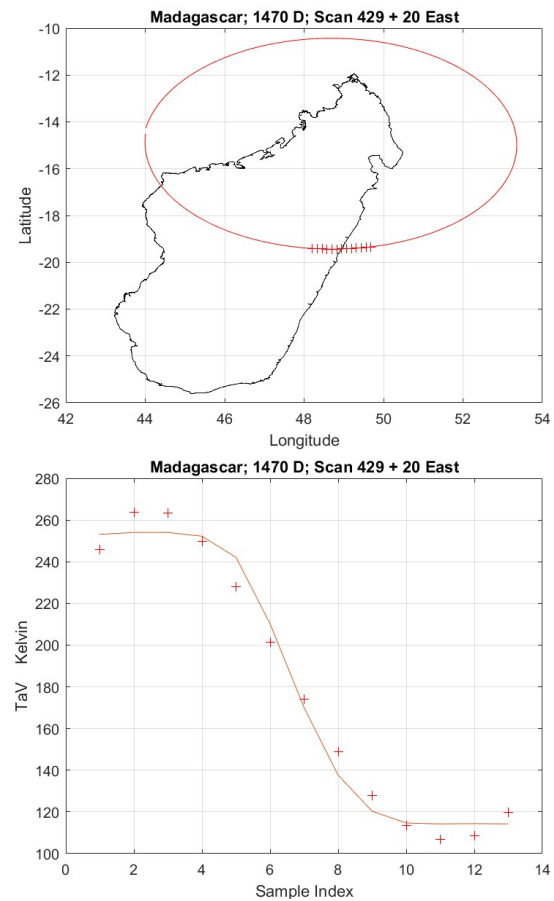


Fig. 1. Geolocation. (Top) SMAP scan across Madagascar. (Bottom) Antenna temperature, TaV. The solid line is a fit to the data samples “+.” The data is for SMAP orbit 01470 D.

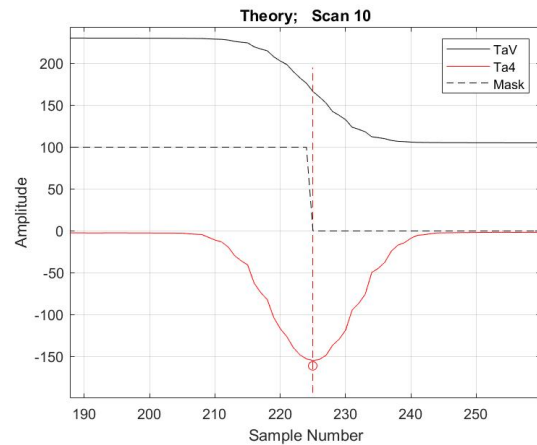


Fig. 2. (Top) TaV and (Bottom) Ta4 at land/water boundary from SMAP simulator. The dashed line is the land mask (water = 0 and land = 100).

Fig. 2. These are curves generated using the SMAP simulator developed at GSFC to support radiometer calibration and study issues such as these [9], [10]. The scene is uniform land on the left and uniform water on the right. The dashed curve indicates the transition from land to water (i.e., the land/water mask). The top curve is the antenna temperature, TaV, calculated with the simulator and the bottom curve is the Ta4 computed with the simulator. In practice, the Ta4 measured by SMAP

is fit with a smooth curve and the peak of the curve is used to identify the coastline. The vertical dashed line through the circle at the peak indicates the coastline in this case. In this ideal case, the estimates from both the inflection point method and the Ta4 method agree and accurately locate the coastline. See [2] for examples of this technique applied to the coastline of Madagascar. In the analysis of data to be presented below the method using Ta4 as described in [2] will be used to locate the boundary.

C. Correcting for Geolocation Error

While the process described above provides a robust estimate of the geolocation error, it does not provide insight into how to correct this error. Knowledge of the geolocation error provides a bound on a potential error in the position of the antenna boresight, but it does not give the information (e.g., the error in the spherical coordinates, θ and φ , defining the antenna boresight vector) needed to correct the pointing error. An error in, θ , is of special importance in passive remote sensing because it impacts knowledge of the incidence angle at the surface. The incidence angle at the ground is a critical parameter in determining emission from the surface and, therefore knowing this angle is important in working backward from the measured antenna temperature to the geophysical parameters of the surface. In the case of SMAP where the antenna spins around the spacecraft z -axis (which is maintained perpendicular to the surface), an error in the scan cone angle, θ , (also called the antenna look angle) is equivalent to an error in the angle the antenna boresight vector makes with the ground.

III. ANALYSIS

The objective of this manuscript is to show how transits at land/water boundaries (i.e., coastlines) with a conical scanning microwave radiometer such as SMAP can be used to identify errors in the coordinates, θ and φ , of the antenna boresight vector with the potential to make corrections to improve the retrieved science product.

A. Introduction

There are many reasons why the radiometer antenna may not be pointing in the position designed: errors in the spacecraft attitude, errors in the antenna deployment, and errors in the antenna itself are some examples. However, in the analysis presented here, it is assumed that the spacecraft attitude is known and that issues of antenna deployment and/or errors in the antenna pattern can be grouped into error in the antenna boresight vector. It is assumed that the spacecraft nadir (z -axis) is aligned with the axis about which the radiometer scans, and that both are pointing perpendicular to the surface. In this case, the antenna boresight vector can be described by spherical coordinates θ and φ about this axis as illustrated in Fig. 3.

In Fig. 3, the antenna boresight vector is specified by polar coordinates θ , which is the cone angle of the scan (also called the antenna “look angle”), and by φ which gives the position

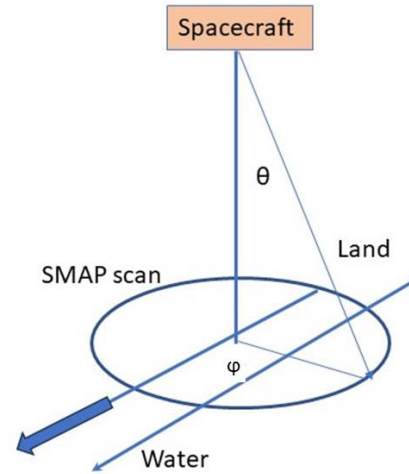


Fig. 3. Antenna boresight geometry.

around the scan (also called azimuth or yaw). In the ideal case, θ is fixed and $\varphi(t)$ gives the position of the boresight vector along the scan. As the scan moves (the SMAP scan is counterclockwise), SMAP reports data at discrete values of $\varphi(t)$ at times $t = tn$ [$n = 0, 1, \dots, 244$]. The coordinates θ and $\varphi(tn)$ determine the location of the SMAP antenna boresight vector (and the location of the centroid of the footprints) on the Earth’s surface as the antenna rotates. Examples of these points on the surface are the “+” in Fig. 1.

B. Geometry

The problem to be addressed here is how to use data obtained with the geolocation algorithm to determine the error in antenna boresight look angle, θ , and azimuth, φ , responsible for the geolocation error. Fig. 4 is an example to illustrate the problem and to show that the errors in geolocation manifest as an apparent error in azimuth. The configuration shown in Fig. 4 is for a positive error in the look angle (actual θ greater than the nominal value) and with no error in φ . The “o” indicates the nominal location of the SMAP footprints: i.e., where the spacecraft data system locates the antenna boresight intersection with the ground. This is where the footprints would be if there was no error. The “+” indicates the actual position of the footprints for each sample. The panel on the top shows the entire scan and the panel on the bottom is an expanded view showing the region near the intersection of the scan with the coastline (the coastline is the straight vertical line along $x = 200$). The radial is a line from the scan origin (spacecraft nadir) to the point near where the actual scan (indicated by the “+”) crosses the boundary.

The scan in Fig. 4 starts at the gap at $x = 0$ (top panel) and rotates counterclockwise. For each “o” there is a corresponding “+.” When there is no error in φ , as in this case, the “o” and “+” are aligned such that a radial at scan position $\varphi(tn)$ passes through an “o” and the corresponding “+.” This can be seen at $x = 0$ in the top panel. In the expanded view in the bottom panel, the “o” and “+” touched by the radial are such a pair.

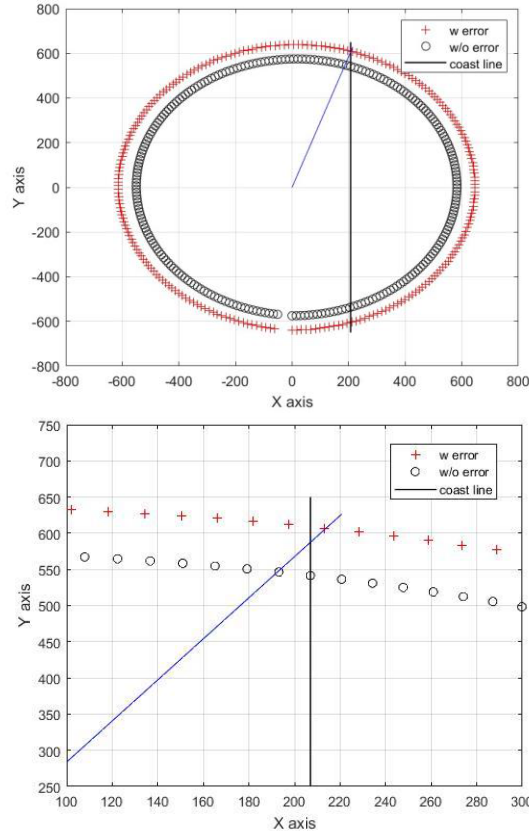


Fig. 4. Scan geometry. The top panel shows the full scan and the bottom panel is an expanded view near the intersection with the land/water boundary. The “o” indicates the nominal (no error) location of the footprints and the “+” indicates the actual positions. The vertical line is the coastline and radial line from the origin indicates a scan position near the intersection with the boundary.

The actual scan (“+”) crosses the boundary at a scan position between the “+” touched by the radial and the next scan position [i.e., between scan positions $\varphi(tn)$ and $\varphi(tn + 1)$]. This is the point that will be found by an accurate geolocation algorithm. But in the nominal spacecraft scan coordinates (“o”) the boundary crossing will be where the boundary (vertical line) intersects the circle along the line near $x = 200$. The geolocation algorithm which uses actual locations, will place the location between the two “+” on either side of the boundary. These scan positions correspond to a point between the first and second “o” to the left of the boundary (i.e., at about $x = 185$). Hence, in the spacecraft coordinates there will be a geolocation error of about 1.5 scan positions to the left of the boundary. That is, in the nominal spacecraft coordinates it will appear that there is a shift of about 1.5 positions in azimuth compared to the expected position.

Because of the way the sensor scans (conical scan) and the way the geolocation is done, all errors in geolocation will manifest as errors in φ . In the example in Fig. 2, there was no error azimuth, the source of the error was an error in look angle, θ , and not φ , but the error manifested as an error in φ . If there were in addition an error in φ , it would have added an offset to the error produced by the error in look angle, and the

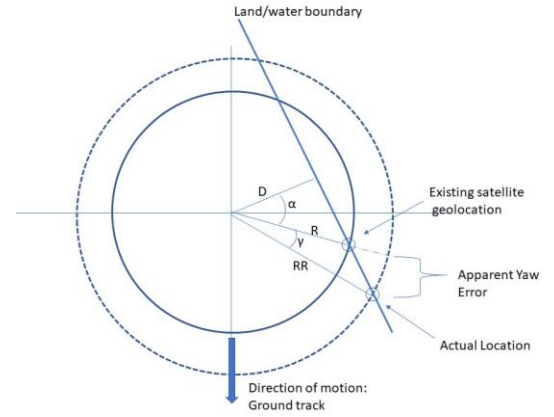


Fig. 5. The figure illustrates the projection of the scan on the ground. The solid circle is the nominal scan and the dashed circle is the actual scan. The small circles indicate the intersection of the nominal and actual scan with the land/water boundary.

combined error would again manifest as an error scan phase, φ . However, the signs of the error at the fore and aft crossing of the boundary are different for errors in look angle and azimuth, and this difference can be used to separate the two and solve for the azimuth and look angle errors themselves. This is described in the section to follow.

C. Solution

The problem is to solve for the azimuth and look for angle errors that produce the error in geolocation. The geometry used to find a solution is shown in Fig. 5 which shows the scan geometry on the ground for the spacecraft shown in Fig. 3. The spacecraft ground track moves along the vertical axis in the direction indicated by the arrow. The land/water boundary is indicated by the solid line. The solid circle indicates the nominal location of the antenna boresight (scan), and the dashed circle indicates its actual location due to an error in the look angle. The location of the actual boundary crossing is indicated by the radial, RR, and the location where the nominal algorithm expects the crossing to occur is indicated by the radial R. The error (the along-scan difference between the two) manifests as an error in azimuth angle, γ . After some straightforward geometry, one finds that

$$\gamma = \arccos(D/RR) - \arccos(D/R) \quad (1)$$

where D is the distance from the scan nadir location (origin in Fig. 5) perpendicular to the boundary. The radii, R and RR , are determined by the spacecraft altitude, H , and the look angle, θ , and look angle error, δ

$$R = H_{\text{eff}}(\theta)\tan(\theta) \quad (2a)$$

$$RR = H_{\text{eff}}(\theta + \delta)\tan(\theta + \delta) \quad (2b)$$

where H_{eff} is an equivalent satellite height that accounts for Earth curvature and a spherical Earth with radius R_e

$$H_{\text{eff}}(\theta) = (H + R_e) - R_e \cos(\beta) \quad (3a)$$

$$\beta(\theta) = \arcsin[(1 + H/R_e)\sin(\theta)] - \theta. \quad (3b)$$

Equation 1 is a parametric equation that gives γ as a function of δ and depends only on altitude, H , and distance D .

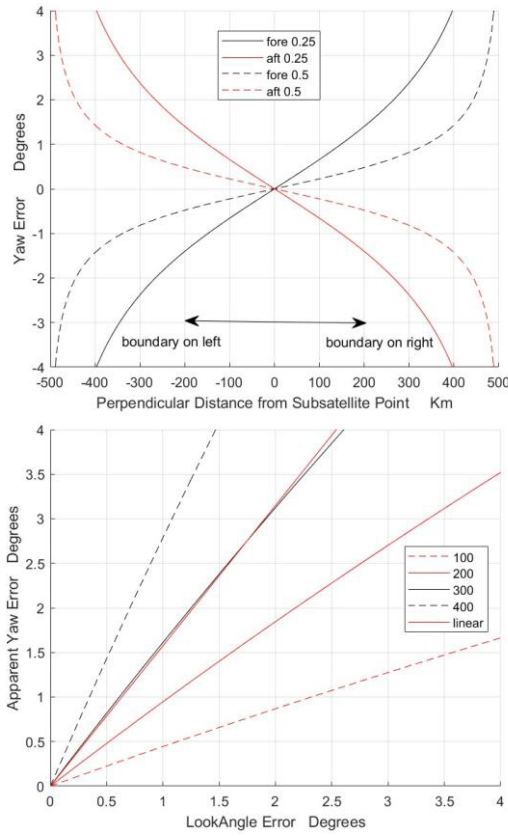


Fig. 6. Graphical solution for look angle error. (Top) Apparent yaw (vertical axis) as a function of distance (horizontal axis) for selected values of look angle error. (Bottom) Apparent yaw (azimuth) as function of look angle error for several values of distance. The red line in the bottom panel labeled “linear” is a straight line fit to the black curve.

Because the scan is a circle, the solution does not depend on the orientation of the coastline relative to the ground track, only its distance, D , from the center of the scan (satellite nadir). This neglects the motion of the spacecraft. However, the motion has a small effect. For example, the time between SMAP footprints is 16.8 ms and the spacecraft velocity is about 7.5 km/s which means the spacecraft moves about 125 m between samples compared to a typical geolocation accuracy of 2 km [1] and the size of the SMAP footprints of about 40 km [5].

Since H is known and D is easily determined given the spacecraft ground track, (1) suggests that if γ can be measured then the error in look angle can be determined. Assuming for the moment that there is no error in azimuth, then γ can be determined directly from the geolocation error (e.g., by converting the geolocation error into degrees along the scan and then solving (1) for the look angle error, δ).

The solution is illustrated graphically in Fig. 6. The panel on the top shows the apparent yaw, γ , in degrees on the vertical axis as a function of distance, D , on the horizontal axis in kilometer for several values of look angle error, δ . In the panel on the bottom, the vertical axis is apparent azimuth (yaw) error and the horizontal axis is look angle error, and the lines are the solution for fixed distance, D . The solution for fixed distance is almost linear (red line) which makes the

solution easy in practice for a known D (i.e., use the straight-line approximation for an analytical relationship between γ and δ).

The discussion above applies when the only error is in the look angle, θ , with no error in azimuth, φ . The opposite case, no error in θ and error only in azimuth, is simple: an error in azimuth is equivalent to a shift of the samples $\varphi(n)$, but no change in the ground path of the scan. In this case, the geolocation algorithm directly identifies the azimuth error after converting distance into degrees along the scan path.

The difficult problem is when there is both look angle and azimuth error. Fortunately, it is possible to separate look angle error and azimuthal error by comparing the boundary crossing of the forward and aft portions of the scan. Using a diagram such as in Fig. 5, it is easy to see that in the case of an error in azimuth, the geolocation error will appear on opposite sides of the land/water boundary (e.g., a shift forward will put the error on the right side of the boundary on the fore portion of the scan and the left side of the boundary on aft crossing of the boundary in the case of a counterclockwise rotation). In the case of a look angle error, the geolocation will appear on the same side of the boundary, on the same side as the satellite nadir for positive error and on the opposite side for negative error. (This will be illustrated with examples in Section IV-A to follow.) Because of this difference in how the errors present themselves, it is possible to separate look angle and azimuth error by adding and subtracting the geolocation error at the fore and aft crossings

$$\text{Az_err} = (\Omega_{\text{fore}} - \Omega_{\text{aft}})\Delta/2 \quad (4a)$$

$$\text{Look_err} = (\Omega_{\text{fore}} + \Omega_{\text{aft}})\Delta/2 \quad (4b)$$

where Ω_{fore} and Ω_{aft} are the measured value of geolocation error in kilometers, Δ is the conversion from km to degrees, and Az_err and Look_err are the apparent yaw errors in azimuth and look angle, respectively. In the case of azimuth, the apparent yaw is also the azimuth error, φ , but in the case of the look angle, the apparent yaw in (4b) becomes the input to (1) which must be solved for the actual error, δ . This can be done, for example, by measuring the distance, D , from the scan nadir perpendicular to the boundary and using the appropriate curve in Fig. 6.

IV. VALIDATION

In this section, the algorithm outlined above will be demonstrated for an ideal land/water boundary using data created with the SMAP numerical simulator. Then it will be tested with real data using SMAP scans over the west coast of Madagascar.

A. Validation Using Data Created With the SMAP Simulator

The SMAP simulator is a numerical code designed to reproduce as closely as possible the signal at the output of the radiometer antenna (i.e., TA). It was originally developed for Aquarius [9], [10] to aid with calibration and is currently used for this purpose with SMAP [11], [12], [13]. It includes a model for emission from the surface, effects of propagation

through the atmosphere and ionosphere to the radiometer, and integration of this signal using the radiometer antenna patterns. The simulator includes the spacecraft ephemeris, effects of the Earth's curvature, and sources of extraneous signal such as the galactic background, Sun glint, and radiation from the Moon. In the application made here, the focus was on the proposed algorithm for retrieving azimuth and look angle error, and the secondary factors such as Faraday rotation and galactic background radiation, normally important for retrievals such as sea surface salinity, were removed. The simulator used a realistic model for surface emission and the SMAP antenna with an ideal linear boundary (straight line) separating ocean and land. The details of the model used for the surface are given in Appendix A.

1) *Simulated Error*: The simulator computed the antenna temperature at the two polarizations, TaV and TaH, and the fourth Stokes parameter, Ta4. Fig. 2 shows an example of the simulated TaV and Ta4. The geolocation was done using the Ta4 as described by [2]. In this geolocation process, the spikes in Ta4 were fit with a polynomial, and the peak was found by setting the derivative of the polynomial to zero. (The data from the simulator does not need to be smoothed in this way, but this was the procedure adopted to handle the noisy, real data from SMAP [2] and was kept here.) By keeping track of the sample numbers [i.e., tn in $\varphi(tn)$] it was possible to place the location of the peak on both the “nominal” scan and also on the scan containing the error.

Fig. 7 is an example of a scan with an azimuthal error but no look angle error. There is only one scan track in this case ($\delta = 0$), but the actual location of the boresight is 2° ahead of the nominal position. The geolocation algorithm locates the boundary correctly (red circle) but because the nominal algorithm is not aware of the error, this algorithm places the location forward by 2° (black circle). The top panel shows the result at the forward crossing and the bottom panel shows the aft crossing. The red “o” is very close to the boundary in both cases, indicating that the geolocation algorithm is working well, but the black circle (where the nominal algorithm locates the boundary) is on opposite sides of the boundary during the fore and aft portions of the scan. As mentioned above, this is characteristic of an azimuth error.

Fig. 8 is an example of a scan with a look angle error of 2° and no error in azimuth. The top panel shows results at the forward crossing and the bottom panel shows the aft crossing. The geolocation algorithm again locates the boundary (red circle) correctly, but this point is on the actual scan which has a slightly larger radius than the nominal scan (e.g., see “+” in Fig. 4 and dashed circle in Fig. 5). In contrast to the case above (azimuth error only, Fig. 7), the nominal algorithm places this point (black “o”) on the same side of the boundary (blue solid line) for both fore and aft crossings. The location would be on the other side of the boundary if the error in θ was negative.

When an error is present in both look angle and azimuth, it is necessary to separate the true error in azimuth from the apparent error (apparent yaw) contributed by the error in look angle. This is done using the algorithm given in (4).

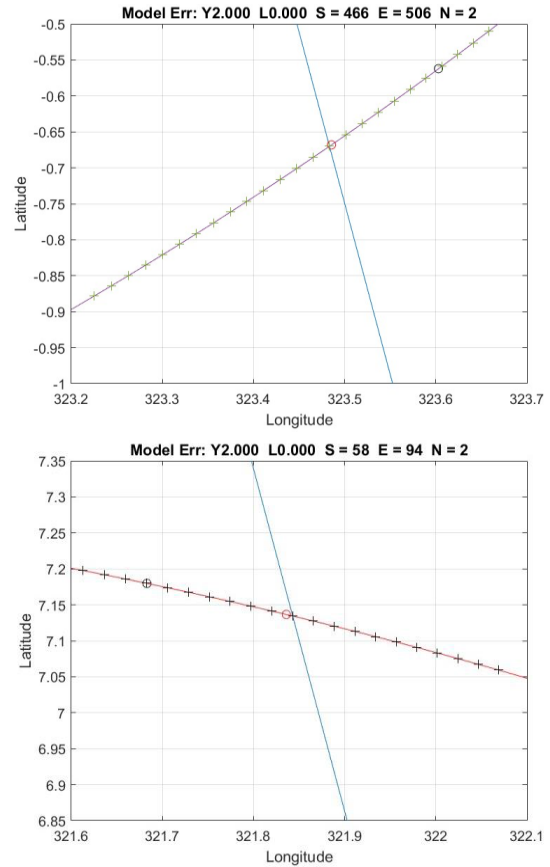


Fig. 7. Azimuthal error only. (Top) Fore crossing. (Bottom) Aft crossing. The blue line is the boundary between (right) land (left) water. The “+” are sample points (footprints) along the orbit, the black “o” is where the spacecraft nominal algorithm locates the boundary and the red “o” is where the geolocation algorithm actual located the boundary. The difference is caused by a yaw of 2° unknown to the nominal algorithm.

2) *Results of the Retrieval Algorithm*: Simulations such as illustrated in Figs. 7 and 8 were performed with several combinations of azimuth and look angle error. The simulator produced Ta4 for the nominal scan and scans with a combination of look angle error, δ , and azimuth error. Then the geolocation algorithm [2] was used to locate the boundary and (4) was used to determine the apparent errors. The azimuthal error is given directly by (4a) and the look angle error is found by using the apparent look angle error from (4b) in (1). As a practical matter, the solution for (1) was obtained by computing D from knowledge of the ground track and fitting the appropriate curve in Fig. 5 (bottom panel) with a straight line. The results are given in Table I.

The first two columns in Table I, labeled “input,” are the errors introduced in the simulator, and the columns labeled “Retrieved” are the values retrieved with the algorithm in (1) and (4). The units are degrees. The retrieved angles are in good agreement with the input with a small residual error. Noise is not included in this simulation, but some error is to be expected because of the finite sample size (1200 samples per scan which corresponds to 0.3° in azimuth) and noise inherent in the geolocation algorithm. On the other hand, the errors are much less than the spacing between the samples even though they are much finer than with the real

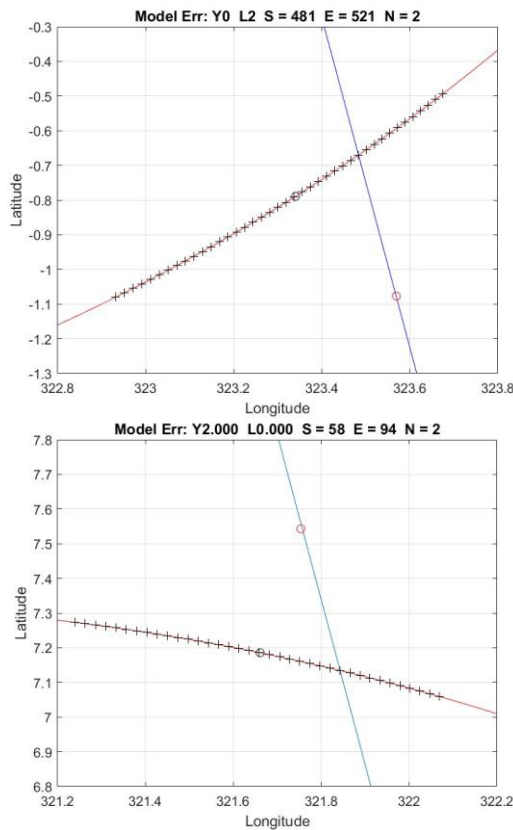


Fig. 8. Look angle error only. (Top) Fore crossing and (Bottom) Aft crossing. The blue line is boundary between (right) land (left) water. The “+” are sample points (footprints) along the orbit, the black “o” is where the nominal algorithm locates the boundary, and the red “o” is where the geolocation algorithm actually located the boundary.

SMAP data. This is again a manifestation of the robustness of the geolocation algorithm which has produced results much better than the size of the radiometer footprint in real SMAP data [1], [2], [3].

B. Application to SMAP Data

The algorithm above was applied to real SMAP data over the east coast of Madagascar (Fig. 1). This is one of the coastlines used in the original geolocation of the SMAP radiometer [1] and later used to validate the Ta4 method for geolocation [2] and is among the coastlines used in a recent revisit to the SMAP geolocation [3].

In this exercise, the half-footprint data from SMAP is used and the boundary was located using Ta4 as outlined by [2]. The SMAP standard footprint is the average of two groups of four data “packets” separated by the time allotted for internal calibration [5], [6]; however, the raw data are available, and it is possible to access the individual data packets. In this exercise, the average of one group of four packets (i.e., half the data in a standard footprint) is used. This is a compromise that gives a factor of two improvement in spatial resolution with a modest (~ 1.4 K) increase in noise.

The east coast of Madagascar is long and reasonably linear, with a minimum of features that would produce inaccuracies

TABLE I
RESULTS FROM THE SIMULATION

Input		Retrieved	
Yaw	Look Angle	Yaw	Look Angle
0	0	0.0495	-0.0115
0	2	0.0225	2.0000
2	0	2.0640	0.0229
1	2	1.0440	1.9427
2	1	1.9920	1.0159
0.25	0.40	0.2865	0.3628
0	-2.0	0.0285	-1.9980

TABLE II
RESULTS FROM SMAP OVER MADAGASCAR

Orbit	Geolocation Difference		Retrieved Error	
	Fore (km)	Aft (km)	Look Angle	Azimuth
1470 D	2.8358	0.5280	0.3304	0.1315
1587 D	-1.0884	2.9212	0.1800	0.2285
1704 D	1.5200	1.8634	0.3323	-0.0196

in geolocation (Fig. 1). There are many SMAP scans with fore or aft crossings of the coastline, but no single scan with both a fore and an aft crossing (because the useful portion of the coastline is a little less than the diameter of the SMAP scans). Instead, the data was partitioned into fore and aft scans and the geolocation data for each set was averaged. The averages were treated as if they came from the same scan and then the algorithm for the retrieval of look angle and azimuth error was applied. The results for three orbits are shown in Table II.

The left column in Table II lists the SMAP orbit used. The middle two columns under “Geolocation Difference” are the results of applying (4) to the raw geolocation data. In this case, the data are in km as given by the geolocation algorithm and have not yet been converted to degrees. The values listed are the average of seven aft crossings and nine fore crossings for each orbit. The “Retrieved Error” is the output of the algorithm in degrees.

V. DISCUSSION

The algorithm for identifying potential error in the antenna boresight vector described in Section III-C above accurately reproduced the errors introduced in the simulated data

(Table I). It was also applied to SMAP data. Unfortunately, there is no absolute way to confirm the results obtained when the algorithm was applied to actual SMAP data (Table II). However, the errors in pointing reported in Table II are consistent with estimates obtained with alternate approaches.

One of these alternatives is the use of the technique of GNSS-R being performed with the SMAP radar receiver [4] to estimate the look angle error. The transmitter on the SMAP radar failed early after launch; however, the receiver is functional and is being used for research on GNSS-R to retrieve surface parameters. Recently, data from the GNSS-R research was used to get an estimate of the pointing angle error by comparing the expected specular point given the spacecraft-source geometry with that observed. The mean value from the three cases in Table II (0.31) is close to the value estimated from the GNSS-R study (≈ 0.25 with variations in time and pointing).

The azimuthal resolution in the study in [4] was not sufficient to report a value for azimuth error. However, an estimate of the azimuth error was reported by [3] using a different approach. In this work, geolocation was done using the inflection point in TA as done in [1], and then a search was made varying the spacecraft ephemeris (pitch, roll, and yaw) and scan cone angle to find errors that minimized the geolocation error. The two largest errors were in yaw (0.15°) and pitch (0.14°). The other errors were much smaller (0.05° and -0.07° for roll and scan cone angle, respectively). The yaw error is equivalent to azimuth error and the value of 0.15° reported in this study [3] is close to the mean of the three values reported in Table II (0.115). Work is underway to test the approach of [3] using the SMAP simulator. The approach is to create an artificial error in antenna pointing using the simulator, then numerically search for errors in spacecraft ephemeris and antenna look angle that minimize the geolocation error.

The accuracy of the technique proposed in this manuscript depends on the accuracy of the geolocation. This depends on finding coastlines that behave like a step function in brightness temperature (i.e., long and straight). The technique also requires both fore and aft crossing which means relatively long boundaries. In the work done here, fore and aft crossings from different scans were averaged. This meant using an average distance to the boundary. Another factor that affects accuracy is the angle the scan makes with the boundary at the crossing. In the ideal case, the scan is orthogonal to the coastline, and the accuracy of the geolocation is degraded when the angle becomes small [2].

The errors in the pointing of the SMAP antenna boresight indicated in Table II are small (as one would expect from a well-designed instrument). The question arises as to whether they are significant. In particular, how much look angle error is tolerable in the context of the requirements on the accuracy of the geophysical parameters, sea surface salinity, and soil moisture, retrieved at L-band. This is primarily a question regarding the error acceptable in look angle which directly impacts emission from the surface. This question is addressed

in Appendix B and the results are presented in Fig. 11. It can be seen from Fig. 11 that errors on the order of 0.2° – 0.3° are important for the retrieval of sea surface salinity where the goal is accuracy of 0.1–0.2 pss, but because the requirements for accuracy in brightness temperature are so much weaker in the case of remote sensing of soil moisture (the goal for SMAP is 4% Mv) errors of 0.2° are not an important concern.

VI. SUMMARY AND CONCLUSION

A method has been proposed to compute look angle and azimuth error in the pointing of the antenna boresight in scanning microwave radiometers such as SMAP. The technique requires a scanning geometry and a high contrast boundary such as land/water and the presence of crossings in both the fore and aft directions. The technique was demonstrated numerically using the simulator developed for SMAP calibration and was then applied to real SMAP data over the coast of Madagascar. The results are reasonable and consistent with estimates of the antenna boresight pointing error using other approaches such as using GNSS-R with the SMAP radar receiver. Although designed with SMAP in mind, the technique should work for any scanning radiometer over well-defined boundaries with high contrast in brightness temperature.

The approach assumes that the error in pointing the antenna boresight can be described as an error in azimuth and look angle (cone angle of the scan). Separating errors in the spacecraft attitude (pitch, roll, and yaw) from errors in the antenna pointing was not addressed.

APPENDIX A SIMULATOR

The SMAP simulator employed here was originally developed for Aquarius [9], [10] and later modified to fit the parameters of the SMAP radiometer where it is currently used as part of calibration [2], [12], [13]. It is a numerical forward algorithm designed to reproduce the radiation from the scene at the spacecraft and compute the signal at the output of the radiometer antenna (i.e., TA). It includes a model for emission from the surface, effects of propagation through the atmosphere and ionosphere, and integration of this signal by the antenna using the antenna patterns of the radiometer. The simulator includes the spacecraft ephemeris, effects of Earth's curvature, and sources of extraneous signals such as the galactic background, Sun glint, and radiation from the Moon.

In the application made here, a simplified version of the simulator was employed to focus on the geolocation algorithm. Propagation effects such as Faraday rotation and extraneous sources such as the galactic background radiation were removed. The emission from the surface and the integration over the SMAP antenna pattern were retained. In addition, the scene was simplified to a homogenous ocean and uniform land surface separated by a straight-line boundary. Roughness on the ocean (waves) and vegetation on the land were not

TABLE III
PARAMETERS OF MODEL FOR DIELECTRIC CONSTANT OF SOIL

Parameter	Value	Parameter	Value
m_v	20 %	ϵ_s	4.7
α	0.65	ρ_b	1.3
β	1.09	ρ_s	2.65
τ	8.54e-12		
$\epsilon_{fw} = 4.9 + 74.1/(1 + j\omega\tau);$			

included, but realistic models for emission (e.g., temperature and dielectric constant) were used for both ocean and land.

The ocean was assumed to be homogeneous with a temperature $T = 20^\circ\text{C}$, salinity $S = 35$ pss, and windspeed $W = 0$ (no waves). The model used for the dielectric constant was the Meissner and Wentz model of 2004 [15], [16] the same as currently employed in the SMAP salinity retrieval algorithm.

The land was also assumed to be uniform and separated from the ocean by a straight line oriented arbitrarily and about 245 km from the nadir point during the scan. The temperature of the land was $T = 20^\circ\text{C}$ with a volumetric soil moisture of $M_v = 0.2\text{ cm}^3/\text{cm}^3$ and with no vegetation or roughness. The Dobson model [14, eq. (28)] was used for the soil with the parameters given in Table III where $\omega = 2\pi f$ and $f = 1.413\text{ GHz}$ is the frequency.

Fig. 2 in the text is an example of the output of the simulator, showing the TaV and $Ta4$ as the radiometer antenna scans across a land/water boundary together with the land/water mask (dashed line). The resolution of the simulator is 1200 samples per scan. Assuming a spacecraft altitude of 685 km [5] this corresponds to a spacing of about 2.6 km and about 0.3° of scan between samples. This resolution was chosen arbitrarily as a compromise between resolution and computation time. The slight variation of the SMAP antenna pattern along the scan was not included.

APPENDIX B SENSITIVITY TO ERROR IN INCIDENCE ANGLE

The incidence angle at the ground is a critical parameter for determining emission from the surface. Knowing this angle is important in working backward from the measured antenna temperature to the geophysical parameters of the surface such as ocean salinity and soil moisture. However, the accuracy with which this angle needs to be known depends on the geophysical parameter itself and on the requirements for accuracy of that parameter, and this requirement is much different for ocean salinity and soil moisture.

The sensitivity of salinity to incidence angle, $dSSS/dI\text{Ang}$, can be computed by taking the ratio of the sensitivity of TA to incidence angle, $dTA/dI\text{Ang}$, to the sensitivity of TA to salinity, $dTA/dSSS$ and the sensitivity of soil moisture to incidence angle, $dSM/dI\text{Ang}$ can be obtained the

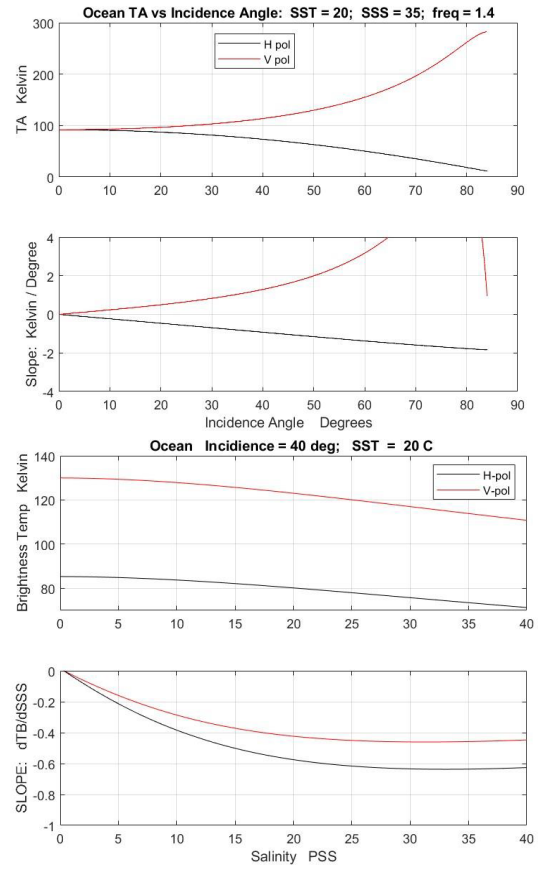


Fig. 9. Sea surface salinity. (Top Panel: top figure) TA as a function of incidence angle. (Top Panel: bottom figure) Derivative of curves in top panel. (Bottom Panel: top figure) TA as a function of salinity. (Bottom Panel: bottom figure) Derivative of curves in the top panel.

same way

$$dSSS/dI\text{Ang} = (dTA/dI\text{Ang}) \div (dTA/dSSS) \quad (5a)$$

$$dSM/dI\text{Ang} = (dTA/dI\text{Ang}) \div (dTA/dSM). \quad (5b)$$

The sensitivities, $dTA/dI\text{Ang}$ and $dTA/dSSS$ or dTA/dSM are straightforward to compute for an ideal flat surface, but they depend strongly on the parameters themselves. Examples are shown in Figs. 9 and 10 for salinity and soil moisture, respectively. In both cases, the surface is ideal (uniform ocean with no waves and uniform land with no roughness and no vegetation canopy). The panel on the top in Figs. 9 and 10 is TA as a function of incidence angle (top) with the derivative $dTA/dI\text{Ang}$ on the bottom. The bottom panel in Figs. 9 and 10 shows TA at the top as a function of SSS (Fig. 9) or SM (Fig. 10) and the derivative $dTA/dSSS$ or dTA/dSM in the bottom sub-panel.

These derivatives vary with polarization and incidence angle and with the parameters SSS and SM themselves. To get an idea of the numbers involved, calculations have been made for 40° incidence (the case for SMAP) for the ocean with $SST = 20^\circ\text{C}$ and $SSS = 35$ pss, and land with $T = 20^\circ\text{C}$ and $SM = 20\%$. The Meissner and Wentz [15], [16] model was used for the dielectric constant of seawater (used by SMAP) and the Dobson model [14] was used for land (see Appendix A). The derivatives for this case have been taken from Figs. 9 and 10 and are given in Table IV.

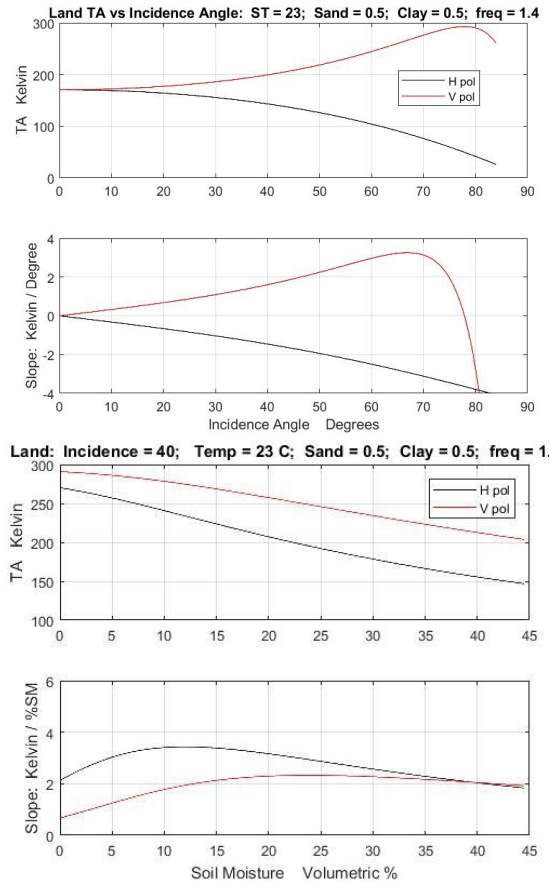


Fig. 10. Sea surface salinity. (Top Panel: top figure) TA as a function of incidence angle. (Top Panel: bottom figure) Derivative of curves in top panel. (Bottom Panel: top figure) TA as a function of salinity. (Bottom Panel: bottom figure) Derivative of curves in the top panel.

TABLE IV
SENSITIVITIES FOR LAND AND OCEAN

Polarization	Ocean			Land		
	dTA/dSSS	dTA/dlAng	dSSS/dlAng	dTA/dSM	dTA/dlAng	dSM/dlAng
Horizontal	-0.46	-0.93	2.02	3.17	-1.46	-0.46
Vertical	-0.64	1.29	-2.01	2.29	1.59	0.69

The significance of the sensitivities computed using the numbers in Table IV are illustrated in Fig. 11. The sensitivities in Table IV have been used to plot the change in soil moisture and salinity as a function of an error in incidence angle: that is, assuming the change is small and using a straight-line perturbation with the slopes given in Table IV. The horizontal axis in Fig. 11 is the error in look angle and the vertical axis is the associated error in soil moisture (left axis) and salinity (right axis). The accuracy requirement for remote sensing of salinity from space is typically 0.2 pss [17]. Hence a small error in look angle has a large impact on remote sensing of salinity. However, this is not the case for remote sensing of soil moisture where the requirement is on the order of 4% (e.g., for SMAP [5]).

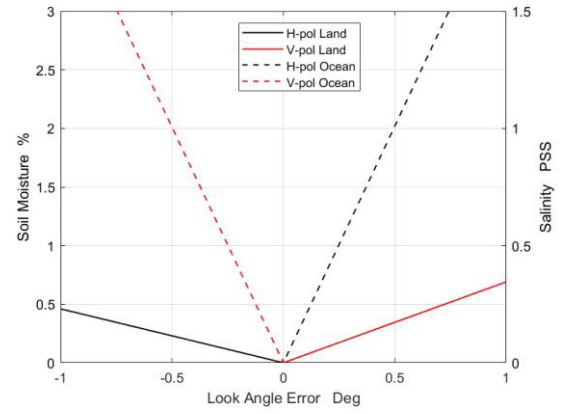


Fig. 11. Effect of error in look angle on soil moisture (solid lines) and ocean salinity (dashed lines). This example is for ocean with SSS = 35 pss and SST = 20 °C and land with SM = 20% Mv and T = 20 °C.

REFERENCES

- [1] G. De Amici, J. Piepmeier, and J. Peng, "Geolocation results for the SMAP passive instrument," in *Proc. 14th Specialist Meeting Microw. Radiometry Remote Sens. Environ. (MicroRad)*, Apr. 2016, pp. 181–185, doi: [10.1109/MICROAD.2016.7530530](https://doi.org/10.1109/MICROAD.2016.7530530).
- [2] D. M. Le Vine, E. P. Dinnat, P. de Matthaeis, and J. Peng, "The fourth Stokes parameter for geolocation in passive microwave remote sensing from space," *IEEE Trans. Geosci. Remote Sens.*, vol. 60, 2022, Art. no. 5305111, doi: [10.1109/TGRS.2022.3215094](https://doi.org/10.1109/TGRS.2022.3215094).
- [3] J. Peng, J. R. Piepmeier, G. De Amici, S. H. Yueh, and D. M. L. Vine, "SMAP radiometer antenna pointing calibration," in *Proc. IEEE Int. Geosci. Remote Sens. Symp. (IGARSS)*, Jul. 2022, pp. 7614–7615, doi: [10.1109/IGARSS46834.2022.9883710](https://doi.org/10.1109/IGARSS46834.2022.9883710).
- [4] J. F. Munoz-Martin, N. Roriguez-Alvarez, S. Yueh, X. Bosch-Lluis, and K. Oudrhiri, "SMAP antenna pointing error estimation using GNSS reflectometry," *IEEE Geosci. Remote Sens. Lett.*, vol. 21, 2023, Art. no. 3503005.
- [5] D. Entekhabi, S. Yueh, P. E. O'Neill, and K. H. Kellogg, *SMAP Handbook*. Pasadena, CA, USA: Jet Propulsion Laboratory, Jul. 2014.
- [6] J. R. Piepmeier et al., "SMAP L-band microwave radiometer: Instrument design and first year on orbit," *IEEE Trans. Geosci. Remote Sens.*, vol. 55, no. 4, pp. 1954–1966, Apr. 2017, doi: [10.1109/TGRS.2016.2631978](https://doi.org/10.1109/TGRS.2016.2631978).
- [7] J. Randa et al., "Recommended terminology for microwave radiometry," Nat. Inst. Standards Technol., United States Dept. Commerce, Washington, DC, USA, Tech. Rep. 1551, Aug. 2008.
- [8] J. R. Piepmeier et al., "Radio-frequency interference mitigation for the soil moisture active passive microwave radiometer," *IEEE Trans. Geosci. Remote Sens.*, vol. 52, no. 1, pp. 761–775, Jan. 2014.
- [9] D. M. Le Vine, E. P. Dinnat, S. Abraham, P. de Matthaeis, and F. J. Wentz, "The aquarius simulator and cold-sky calibration," *IEEE Trans. Geosci. Remote Sens.*, vol. 49, no. 9, pp. 3198–3210, Sep. 2011, doi: [10.1109/TGRS.2011.2161481](https://doi.org/10.1109/TGRS.2011.2161481).
- [10] E. P. Dinnat, D. M. Le Vine, J. R. Piepmeier, S. T. Brown, and L. Hong, "Aquarius L-band radiometers calibration using cold sky observations," *IEEE J. Sel. Topic Appl. Earth Observ. Remote Sens.*, vol. 8, no. 12, pp. 5433–5449, Dec. 2015, doi: [10.1109/JSTARS.2015.2496362](https://doi.org/10.1109/JSTARS.2015.2496362).
- [11] E. P. Dinnat and D. M. L. Vine, "SMAP calibration using cold sky observations," in *Proc. IEEE Int. Geosci. Remote Sens. Symp.*, Kuala Lumpur, Malaysia, Jul. 2022, pp. 4236–4239, doi: [10.1109/IGARSS46834.2022.9884569](https://doi.org/10.1109/IGARSS46834.2022.9884569).
- [12] J. Peng et al., "Soil moisture active/passive L-band microwave radiometer postlaunch calibration," *IEEE Trans. Geosci. Remote Sens.*, vol. 55, no. 9, pp. 5339–5354, Sep. 2017, doi: [10.1109/TGRS.2017.2705342](https://doi.org/10.1109/TGRS.2017.2705342).
- [13] J. Peng et al., "Soil moisture active/passive (SMAP) L-band microwave radiometer post-launch calibration upgrade," *IEEE J. Sel. Topics Appl. Earth Observ. Remote Sens.*, vol. 12, no. 6, pp. 1647–1657, Jun. 2019, doi: [10.1109/JSTARS.2019.2902492](https://doi.org/10.1109/JSTARS.2019.2902492).
- [14] M. Dobson, F. Ulaby, M. Hallikainen, and M. El-rayes, "Microwave dielectric behavior of wet soil—Part II: Dielectric mixing models," *IEEE Trans. Geosci. Remote Sens.*, vol. GE-23, no. 1, pp. 35–46, Jan. 1985, doi: [10.1109/TGRS.1985.2894](https://doi.org/10.1109/TGRS.1985.2894).
- [15] T. Meissner and F. J. Wentz, "The complex dielectric constant of pure and sea water from microwave satellite observations," *IEEE Trans. Geosci. Remote Sens.*, vol. 42, no. 9, pp. 1836–1849, Sep. 2004.

- [16] T. Meissner and F. J. Wentz, "The emissivity of the ocean surface between 6 and 90 GHz over a large range of wind speeds and earth incident angles," *IEEE Trans. Geosci. Remote Sens.*, vol. 50, no. 8, pp. 3004–3026, Aug. 2012.
- [17] G. S. E. Lagerloef, C. T. Swift, and D. M. L. Vine, "Sea surface salinity: The next remote sensing challenge," *Oceanography*, vol. 8, no. 2, pp. 44–50, 1995.



David M. Le Vine (Life Fellow, IEEE) received the Ph.D. degree in electrical engineering from the University of Michigan, Ann Arbor, MI, USA.

His background is electrical engineering with specialization in electromagnetic theory and physics. He did his research at the Earth Sciences Division, National Aeronautics and Space Administration (NASA) Goddard Space Flight Center, Greenbelt, MD, USA, where he works to develop techniques for microwave remote sensing of the environment from space. Examples of this work are the development

of the synthetic aperture radiometer, ESTAR, and the launch of AQUARIUS, a NASA Earth System Science Pathfinder (ESSP) mission to measure SSS. He was the Deputy Principal Investigator for AQUARIUS. He is a member of the Ocean Salinity Science Team which continues research on remote sensing of SSS. He is also a member of the science team for NASA's Soil Moisture Active Passive (SMAP) mission and the Quality Working Group supporting European Space Agency (ESA) Soil Moisture and Ocean Salinity (SMOS) mission. His teaching experience includes the Department of Electrical Engineering, University of Maryland, College Park, MD, USA, and an Adjunct Faculty with The George Washington University, Washington, DC, USA. His current research is on passive remote sensing at the long wavelength end of the microwave spectrum (e.g., L-band) with applications to remote sensing of soil moisture and sea surface salinity (SSS).

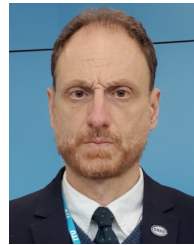
Dr. Le Vine is a member of GRSS, Antennas and Propagation Society, the International Union of Radio Science (URSI), and American Geophysical Union. He was a recipient of the IEEE/GRSS Distinguished Achievement Award in 2016 and the Golden Florin Award in 2014 for contributions to microwave radiometry. He has served on the Geoscience and Remote Sensing Society (GRSS) AdCom and several IEEE committees focused on engineering accreditation.



Emmanuel P. Dinnat (Senior Member, IEEE) received the Advanced Studies degree in instrumental methods in astrophysics and spatial applications and the Ph.D. degree in computer science, telecommunications, and electronics from University Pierre and Marie Curie, Paris, France, in 1999 and 2003, respectively.

He is a Research Scientist with the Cryospheric Sciences Laboratory, NASA Goddard Space Flight Center (GSFC), Greenbelt, MD, USA. He has been working on the calibration, retrieval algorithm

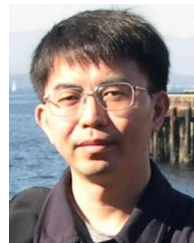
development, and science product validation for various airborne experiments and satellite missions. His research interests include active and passive microwave remote sensing, sea surface salinity, scattering from rough surfaces, atmospheric radiative transfer, and numerical simulations. His latest research focuses on high-latitude oceanography and the interactions between the cryosphere and oceans.



Paolo de Matthaeis (Senior Member, IEEE) received the Laurea degree (summa cum laude) in electrical engineering from the University of Rome "Tor Vergata," Rome, Italy, in 1991, and the D.Sc. degree in electrical engineering from George Washington University, Washington, DC, USA, in 2005.

After graduation, he was with European Space Agency, ESTEC, Noordwijk, The Netherlands, under the Young Graduate Trainee Program, and then with the Remote Sensing Laboratory, University of Rome "Tor Vergata." He started working with the NASA Goddard Space Flight Center, Greenbelt, MD, USA, as a Research Associate, where he is currently a Senior Research Engineer. He was part of the Science Algorithms Calibration/Validation Team for the Aquarius instrument and is now part of the team working on sea surface salinity estimation using SMAP. His research interests include active and passive microwave remote sensing, with a focus on electromagnetic modeling of vegetation, land, and sea surface, and detection and mitigation of radio frequency interference (RFI).

Dr. de Matthaeis is a member of U.S. National Committee (USNC) for URSI. He is a member of the IEEE Geoscience and Remote Sensing Society (GRSS) and has been active in the Frequency Allocations in Remote Sensing Technical Committee (FARS-TC). He is currently the Chair of the FARS-TC and has been the Chair or the Co-Chair since 2017.



Jinzheng Peng (Senior Member, IEEE) received the B.S. degree in electrical engineering from Wuhan University, Wuhan, China, the M.S. degree in electrical and computer engineering from the University of Massachusetts, Amherst, MA, USA, and the Ph.D. degree in electrical engineering from the University of Michigan, Ann Arbor, MI, USA.

From 1991 to 2000, he was with Beijing Institute of Remote Sensing Equipment, Beijing, China. He is currently with the Goddard Earth Sciences Technology and Research (GESTAR), Morgan State

University, Baltimore, MD, USA, and also with the NASA's Goddard Space Flight Center, Greenbelt, MD, USA. He is currently working on algorithm development and calibration/validation for the Soil Moisture Active/Passive (SMAP) radiometer. His research interests include system-level concept design, analysis, calibration/validation, and algorithm development for microwave remote-sensing instruments.